engineering proceedings

MDPI

Proceeding Paper

A Computational Multiphysics Study of a Satellite Thruster †

Marcello A. Lepore [1,*], Marzio Piller [1], Mario Guagliano [2] and Angelo R. Maligno [3]

[1] Department of Engineering and Architecture, University of Trieste, 34127 Trieste, Italy; piller@units.it
[2] Department of Mechanical Engineering, Polytechnic University of Milan, 20156 Milan, Italy; mario.guagliano@polimi.it
[3] Institute for Innovation in Sustainable Engineering, College of Science and Engineering, University of Derby, Derby DE1 3HD, UK; a.maligno@derby.ac.uk
* Correspondence: marcello.lepore@dia.units.it
† Presented at the 53rd Conference of the Italian Scientific Society of Mechanical Engineering Design (AIAS 2024), Naples, Italy, 4–7 September 2024.

Abstract: This work concerns a study of the thermomechanical behaviour of a commercial thruster for aerospace use. The thruster, operated using a bipropellant liquid mixture, is used for the motion and in-orbit altitude control of small telecommunications satellites. The mixture used in the combustion process is composed of propylene and nitrous oxide, while the wall of the thruster is made of PH15-5 stainless steel. A computational fluid dynamics analysis of conjugate heat transfer determines the spatial–temporal distribution of temperature within the thruster wall. This information is passed to a finite element mechanical model that simulates the stress and the equivalent plastic strain distribution within the thruster wall.

Keywords: aerospace thruster; liquid propellant; thermal-stress analysis

Academic Editors: Umberto Galietti, Gabriele Arcidiacono, Enrico Armentani, Davide Castagnetti, Vigilio Fontanari, Aurelio Somà and Nicola Bonora

Published: 14 February 2025

Citation: Lepore, M.A.; Piller, M.; Guagliano, M.; Maligno, A.R. A Computational Multiphysics Study of a Satellite Thruster. *Eng. Proc.* **2025**, *85*, 14. https://doi.org/10.3390/engproc2025085014

1. Introduction

Over the last decade, several studies based on numerical simulations have been performed to evaluate both the combustion process and the thermomechanical behaviour of thrusters for aerospace use [1–8]. Small-satellite and thruster solutions have been proposed [9–12], despite severe limitations in their functionality inherent to their limited mass and volume, as they turn out to be economically convenient compared to traditional satellites, which have the disadvantage of having high launch vehicle costs. In addition, a thrust of a few Newtons may be sufficient to move small satellites into orbit, and this depends on the orbital position, on the vehicle's weight and on the needs of the mission [13,14]. In general, in thrusters for aerospace use, the nozzle is also a critical component as it allows the expansion and acceleration of the gases produced in the propellant combustion process. Any structural failure in this component directly translates into a loss of thrust. Therefore, material selection and structural analysis are critical moments in the design of these components [15]. Combustion chambers and nozzles work in extreme conditions with combustion product temperatures reaching or exceeding 3000 K, with variable pressures up to 3 MPa and supersonic flow speeds. The temperatures of both the combustion chamber and the nozzle increase very rapidly after ignition of the propellant, and therefore, the thermal shock makes the inner wall of the thrusters susceptible to erosion and cracking [16,17]. Thermochemical erosion by oxidising species of combustion products [18] and combustion instabilities [19,20] significantly accelerate this process. Above all, the nozzle throat represents one of the most critical parts. Therefore, a simulation of the combustion process followed by a thermomechanical analysis for the evaluation of the material behaviour of the thruster is fundamental in the design phase [21]. In this study, the thruster under investigation is a 20N class bipropellant rocket engine developed by the ATLAS consortium (ATLAS—Advanced Design of High-Entropy Alloys Based Materials for Space Propulsion, Horizon 2020). The thruster used nitrous oxide (N_2O) as an oxidiser and propylene (C_3H_6) as fuel. These are so-called green propellants [22–27], which means they are non-toxic and are relatively safe to use compared to conventional rocket propellants. Furthermore, these propellants are self-pressurising, which means that their vapour pressure in saturation conditions is high enough to act as supply pressure. Thus, a separate pressurised gas or a mechanical pressurisation system is not required to drive the propellants to the combustion chamber. The thruster is currently made of Inconel or PH15-5 stainless steel and can work for a maximum duration of approximately 10 s before thruster cooling is required to prevent overheating. In many cases, this time would be enough to guarantee the correct functioning of the thruster; however, a longer operating time could be required to carry out more complex manoeuvres in orbit, and therefore, it would be necessary to increase the combustion time. In view of the above, the material used for the thruster's wall must resist intense thermo-mechanical stresses as well as corrosion by nitrous oxide and its combustion products in combination with propylene. Thus, in this work, the modelled B20 thruster does not integrate a cooling system, and the authors want to demonstrate that it is possible to study the thermo-mechanical behaviour of the thruster in the thermal transient using a finite element mechanical model by introducing one-dimensional heat flux on the inner part of the thruster wall in a specific time. This heat flow is obtained at equilibrium of the combustion process in a CFD analysis. Subsequently, the initial heat flux is scaled with a heat flux decay law calculated with CFD analysis. To validate the mechanical model, a comparison of the temperature fields on the inner wall of the thruster calculated with CFD and finite element analysis is carried out. The proposed investigation provides a baseline for future improvements to the B20 thruster, aimed at prolonging its operating time while preventing structural damage.

2. Geometry

A 3D CAD model of the B20 thruster without a cooling system was provided by the ATLAS consortium, and the cooling system is a radiation-cooled thrust chamber. As shown in Figure 1, on the outside, a perforated anchoring plate for the thruster and the covering of the propulsion unit are highlighted. Two independent toroidal-shaped distribution rings collect the fuel and the oxidiser, respectively, which are fed therefrom to the combustion chamber through fifteen inclined injection ducts, distributed in five groups of three injectors each—two for the oxidiser, one for the fuel—as shown in Figure 1.

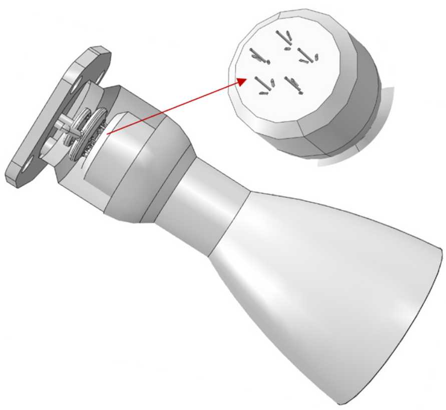

Figure 1. Three-dimensional geometry model of B20 thruster with main components highlighted.

The injectors conveying the oxidiser are inclined by 70° to the symmetry axis of the thruster and lie on radial planes. This configuration has proven particularly suitable in small-sized thrusters as it can increase the turbulence produced during the combustion of the mixture. Figure 2 presents a 2D representation of the thruster. The thruster has an overall length of 0.09 m, while the wall thickness is non-uniform along the thruster with a maximum value of 0.0045 m corresponding to the combustion chamber. Finally, the diameter of the nozzle throat is 0.01 m.

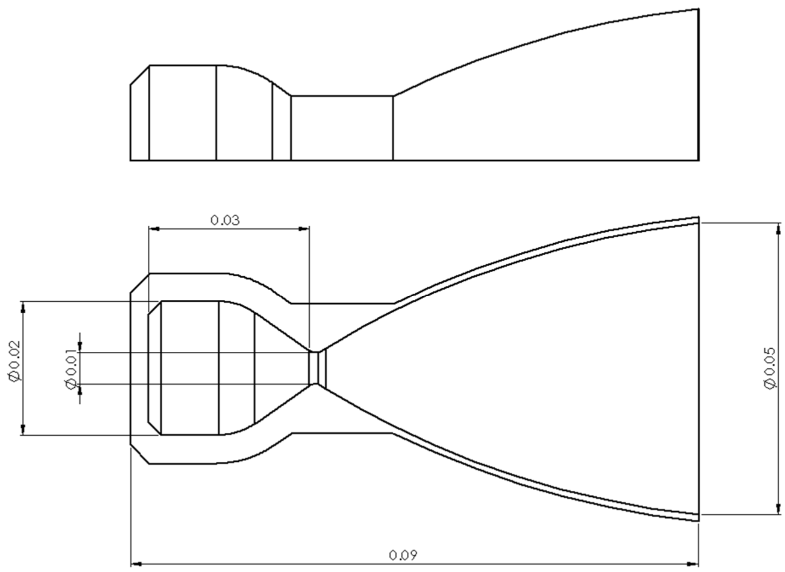

Figure 2. Geometry and dimensions (m) of B20 thruster.

3. Materials and Methods

The thruster was built with PH15-5 H1100 stainless steel, specifically intended for high-temperature applications. PH15-5 is a martensitic steel with mechanical properties particularly suitable to produce small thrusters. PH15-5 is a steel that initially had an austenitic microstructure which, following heat treatment, evolves into a martensitic microstructure. Specifically, the heat treatment was performed in an oven for four hours at a constant temperature of 593 °C (1100 °F) followed by air cooling. Furthermore, the thruster was obtained using additive technologies through a Selective Laser Melting (SLM) process. Therefore, the thruster was built in layers, starting from the fusion of a bed of very fine-grained metal powder. The mechanical properties of PH15-5 H1100 were provided by the ATLAS consortium, as reported in Table 1, and refer to parts produced with Additive Manufacturing (AM). Both the mass density and the specific heat were independent of temperature in the reported simulations.

Table 1. PH15-5 H1100 material data.

Young's Modulus [GPa]	Poisson's Ratio [-]	T [K]	Plastic [GPa]	Strain [-]	T [K]	Density [kg/m^3]
196	0.27	300	0.246	0	300	7800
183	-	422	0.544	0.49	300	-
165	-	500	0.153	0	600	-
147	-	588	0.433	0.49	600	-
113	-	773	0.1319	0	900	-
94.1	-	800	0.330	0.49	900	-

Table 1. *Cont.*

Young's Modulus [GPa]	Poisson's Ratio [-]	T [K]	Plastic [GPa]	Strain [-]	T [K]	Density [kg/m^3]
75.1	-	973	0.125	0	1200	-
42.9	-	1173	0.158	0.49	1200	-
Linear Expansion Coefficients [m/m K]	**T [K]**	**Conductivity [W/m K]**	**T [K]**	**Specific Heat [J/kg K]**		**T [K]**
1.13×10^{-5}	294	18.25	300	420		300
1.17×10^{-5}	366	19.65	400	-		400
1.19×10^{-5}	477	22.3	600	-		600
1.22×10^{-5}	589	24.89	800	-		800
1.22×10^{-5}	774	30.82	1200	-		1200

Reference data for the mass flow rates of fuel and oxidiser entering the combustion chamber and for the rocket thrust were taken from the technical data sheet of the B20 propulsor.

3.1. The CFD Model

Taking advantage of the axial symmetry of the thruster's geometry, a 2D model of the B20 thruster was created with the wall thickness and shape following the actual geometry of the 3D model. After a thorough convergence study, the final geometry of the CFD model was meshed with 150,000 quadrilateral linear elements, where the minimum edge length was 4×10^{-4} m. A commercial software for fluid dynamic analysis was used to simulate the combustion process. From this simulation, the heat fluxes, pressures and shear stresses on the inner wall of the B20 thruster were calculated. To simulate the combustion process, a PDF table was built using lookup tables [28]. The parameters and values reported in Table 2 were introduced into the lookup tables to model the combustion process of the liquid mixture.

Table 2. Parameters and values to model the combustion process.

Parameters	Values
Fuel Stream Rich Flammability Limit (stoichiometric 0.18)	0.36
Gauge Pressure—Inlet Fuel—C_3H_6	1,470,000 Pa
Gauge Pressure—Inlet Oxidiser—N_2O	7,200,000 Pa
Temperature—Inlet Fuel	300 K
Temperature—Inlet Oxidiser	300 K
Operating Equilibrium Pressure	100,000 Pa
Outlet Pressure	0 Pa

The K-ε model is one of the most common turbulence models. It is a two-equation model, which means it includes two extra transport equations to represent the turbulent properties of the flow. It is also appropriate to consider that in the 2D model of the thruster proposed in this work, the propellant mixture was introduced through inlets that have an area equal to that reported in the 3D CAD model. Hence, the lookup tables were built starting from the percentage of the mole fraction composition of the combusted gases during the ignition time provided by ATLAS consortium. As previously stated, propylene (C_3H_6) and nitrous oxide (N_2O) were used as the fuel and oxidiser, respectively. Propylene is considered a green propellant because, if burned, it theoretically should not produce

NOx. However, this statement is true only if the decomposition of propylene occurs at a minimum temperature of 900 °C. In this study, the temperatures were high enough to enable the complete decomposition of propylene. Moreover, it is worth noting that the possible presence of NOx would be irrelevant for the calculation of heat fluxes.

3.2. CAD Model for Thermo-Structural Analysis

The CAD model of the B20 thruster without a cooling system was imported into a commercial software based on the FE. The model was subsequently partitioned and discretised using the FE code. Then, the model was meshed with 166,320 quadratic hexahedral elements with reduced integration, for thermo-structural analyses. As the model of the rocket is axisymmetric, a quarter of the full model was used when simulating thermomechanical behaviour. Hence, both the symmetry conditions on cutting planes and constraints on the external surface of the combustion chamber, to prevent rigid body degrees of freedom, were applied (see Figure 3).

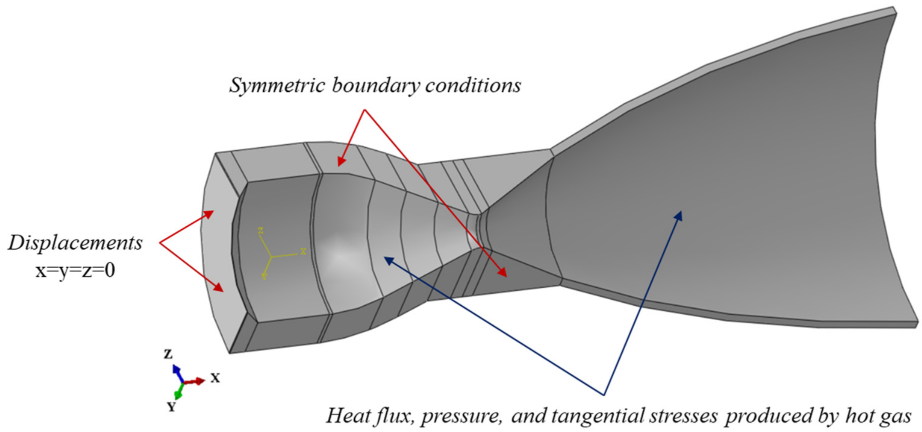

Figure 3. The boundary and load conditions applied in the mechanical model of the thruster.

Moreover, on the external surface of the thruster, another boundary condition related to radiative heat exchange towards the environment was applied. In this latter case, emissivity was established by the ATLAS consortium and set to 0.8. The heat fluxes, pressures and tangential stresses produced by the burnt gases, varying along the thruster axis, were applied on the inner surface of the thruster (see Figure 3). Hence, the thermomechanical analysis was carried out in three sequential steps. The first step related to the ignition phase, which ended in a time of 0.05 s. The second step related to the heating of the wall in a maximum time of ten seconds from the end of ignition. The third step related to the shutdown time, which was equal to 100 ms.

3.2.1. Operating Cycle

CFD simulation of the combustion process of the liquid mixture allowed the calculation of convective heat fluxes, pressures and shear stresses on the boundary of the fluid control volume. Therefore, these loading conditions were considered to enter through the inner wall surface of the 3D mechanical model. Therefore, the thermal-stress analysis was carried out considering the thermal and nonlinear transient behaviour of the wall material with the operating cycle defined by the ATLAS consortium. A qualitative representation of the cycle is shown in Figure 4. Initially, a uniform temperature of 298 K was applied to the wall. Next, convective heat fluxes, pressures and shear stresses were applied along the length of the thruster by three field functions defined in the FE commercial code.

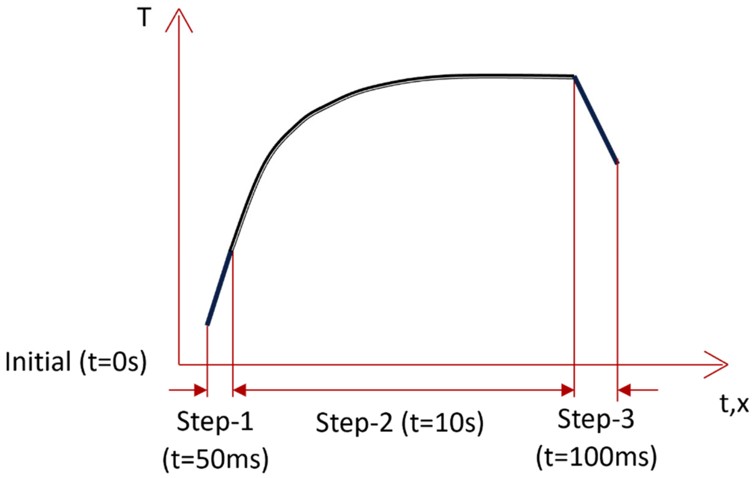

Figure 4. Operating cycle.

Three consecutive steps were used to define the thermal cycle described in Figure 4. Step 1 related to the onset of combustion, when the maximum values of heat fluxes, pressures and shear stresses were applied on the inner surface of the wall during the first 50 ms. In step 2, the wall of the thruster was heated up by conduction up to a maximum time of 10 s, and finally, in step 3, the shutdown of the thruster (100 ms) was modelled by removing all the loads previously applied.

3.2.2. The Law of Decay of Heat Flux

The maximum value of the wall heat flux was calculated along the longitudinal axis (*X*-axis) of the thruster. This point of maximum heat flux was found at the nozzle throat. Subsequently, the heat flux values at different instants of time up to 10 s were calculated at this throat location. These values were plotted on a heat flux-versus-time graph, as shown in Figure 5. Interpolation of these values permitted us to obtain the lowest point of decay of heat flux. Indeed, the heat flux values decay over time because heat flux coefficients decay over time. In Figure 5, it is worth noting that the behaviour of heat flux over time is quite oscillating. This behaviour is related to some pressure oscillations within the volume of the burnt gas. Hence, the law of decay of heat flux can be obtained through the interpolations of data reported in Figure 5 with a power law. The use of a power law can permit us to quickly simulate the heat flux decay in the mechanical model.

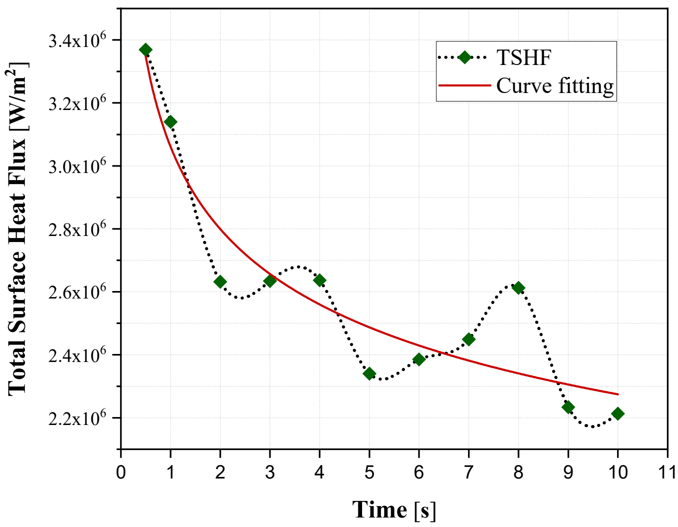

Figure 5. Each dot (green) represents a heat flow value over time, calculated in the nozzle throat. The interpolation curve (red) highlights a decay law of the heat flux.

The equation of the power law shown in Figure 5, y = 3 × 10^6 $a^{-0.127}$, was used to calculate the decay of the heat fluxes on the inner wall of the thruster over time. It is worth noting that a stationary condition appeared at two seconds from the start of the burn.

4. Results and Discussion

The CFD analysis was carried out considering a two-dimensional model of the thruster. Furthermore, the percentage composition of the mole fraction of the flue gases provided by the ATLAS consortium was used to write the lookup tables. The CFD analysis also returned the temperature distribution within the thruster's wall. Then, the temperature distribution on the inner surface of the wall along the axial direction was compared with that obtained from the mechanical model. In Figure 6, the temperature distribution within the fluid volume and wall is shown at 50 milliseconds.

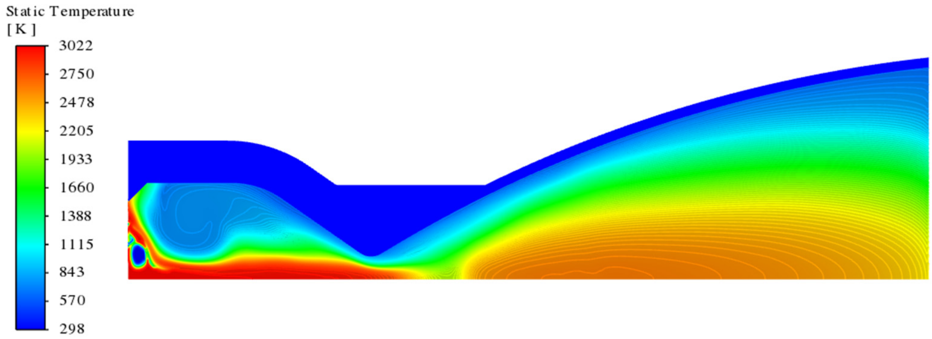

Figure 6. Temperature distribution at the start of combustion (50 ms).

The wall heat flux q was applied along the X-direction, in the nozzle throat, at a distance equal to x = 0.026 m from the mixture inlets (x = 0.0 m). In Figure 7, the temperature distribution along the *X*-axis at 2 s is shown.

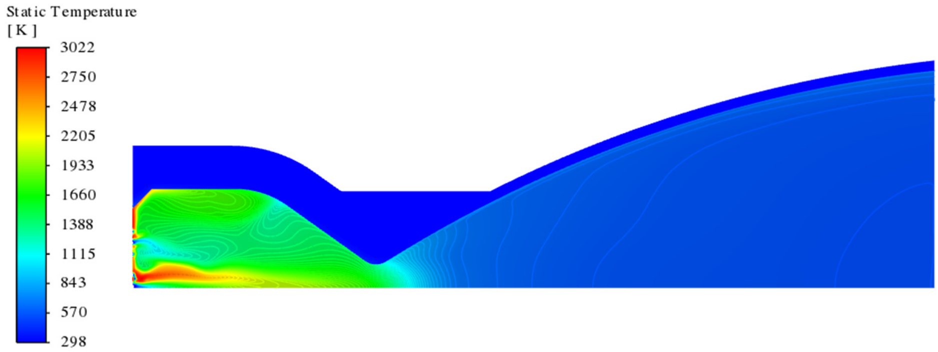

Figure 7. Temperature distribution at the beginning of combustion (2 s).

In Figure 8, the temperature field inside the thruster is shown after 10 s from the start of the combustion.

These temperature fields, relating to different instants of time, were compared with the corresponding temperature fields obtained from the thermo-mechanical analysis carried out with the 3D mechanical model (see Figure 9). Looking at the graph shown in Figure 9, the differences between the temperature values calculated by the CFD analysis and those correlated to the power law, used to interpolate the points shown in Figure 9, highlight a maximum difference in the order of 6%. Thus, the proposed approach is considered acceptable.

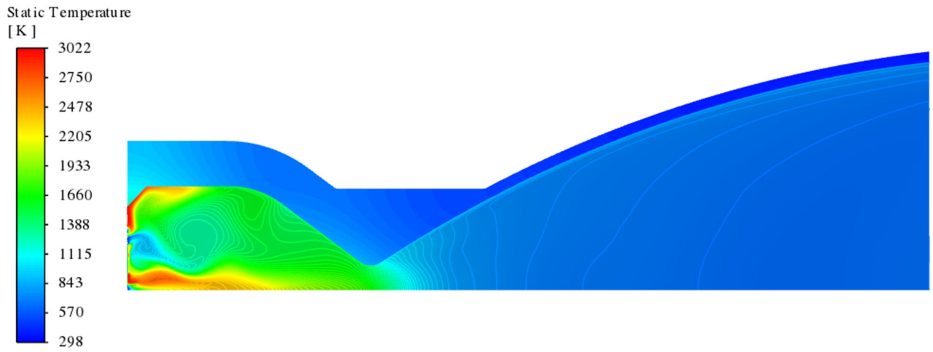

Figure 8. Temperature distribution at the end of combustion (10 s).

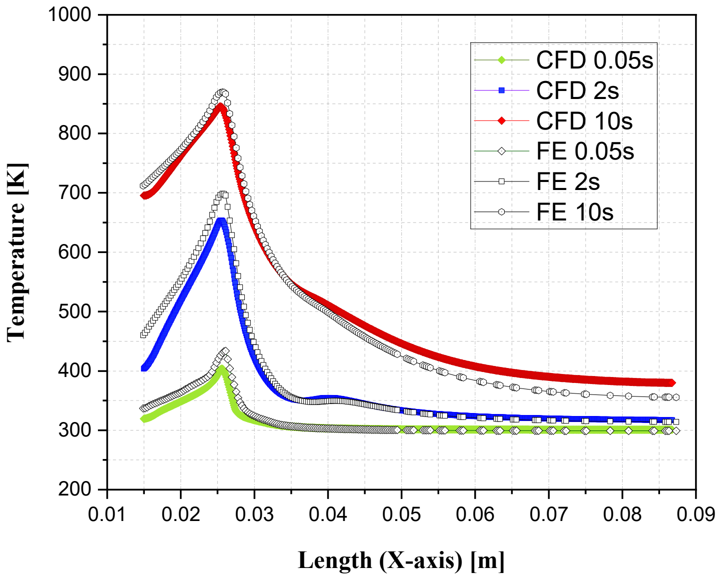

Figure 9. A comparison of temperature profiles over time on the inner surface of the thruster and along the *X*-axis.

Thermal-Stress Analysis

The elastoplastic properties were used to model the material behaviour of the thruster wall. These material properties were introduced into the mechanical model in the form of a bilinear law, as reported in Table 1, and for different values of temperature, adopting the elastoplastic von Mises criterion and isotropic hardening. Heat flux, von Mises stress, plastic strain, total strain, thermal strain (THE) and equivalent plastic strain (PEEQ) were also calculated through nonlinear thermal–structural analysis. This work demonstrated that the maximum peaks of heat fluxes, temperatures, von Mises stresses and, finally, inelastic deformations were found in the nozzle throat region. In Figure 10, the maximum value of PEEQ in the wall at two seconds is shown. By observing the PEEQ, it is possible to identify the most damaged area of the thruster wall.

It is worth noting that two seconds into combustion, there is no numerical evidence that plastic strain has increased. Since total strain is the sum of thermal strain and mechanical strain, total strain can be written as the sum of elastic strain, inelastic strain and thermal strain. Furthermore, inelastic deformation is the sum of plastic deformation and viscous deformation and was not considered in this work.

Therefore, the plot of equivalent strain, PEEQ, shows the amount of plasticity in the nozzle throat in relation to the total strain and, therefore, due to both mechanical and thermal loading. However, considering equivalent plastic strain and thermal strain separately, most of the plasticity is related to thermal strain.

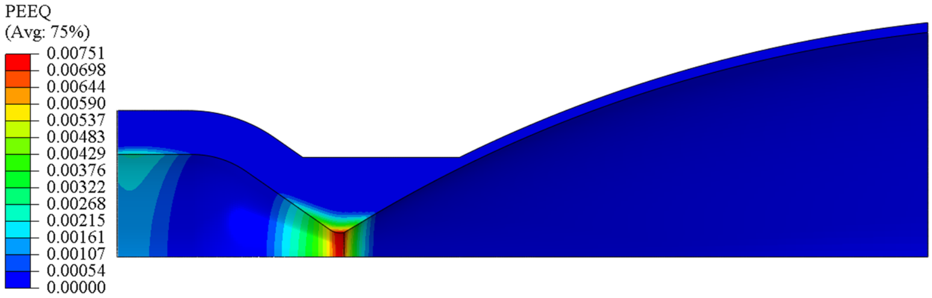

Figure 10. An image highlighting the most damaged region in the nozzle throat of the thruster at 2 s.

5. Conclusions

An explicit CFD analysis was performed to model both the combustion process of a liquid propellant and to calculate the heat fluxes on the inner surface of the wall of a commercial thruster. Then, the heat fluxes were used to calculate the temperature field in the thruster wall in the thermal transient. Subsequently, using a heat flow decay law calculated at the end of the CFD analysis, a mechanical model of the thruster was used to perform an implicit thermomechanical analysis considering the properties of the elastoplastic material. The procedure proposed in this work allowed us to identify the regions of the wall that were most damaged by the thermomechanical load and therefore most critical for its operation under thermal shock conditions. Furthermore, this procedure can allow us to compare the thermomechanical behaviour of the thruster wall using different materials without having to repeat the CFD analysis, assuming that for these materials, the difference in the values of thermal conductivity is negligible. Finally, this approach can be used as a starting point for the analysis of the fatigue behaviour of the thruster wall.

Author Contributions: Conceptualization, M.A.L.; methodology, M.A.L.; software, A.R.M.; validation, A.R.M., M.G. and M.P.; formal analysis, M.A.L. and M.P.; investigation, M.A.L.; resources, A.R.M.; data curation, M.A.L.; writing—original draft preparation, M.A.L.; writing—review and editing, M.A.L. and M.P.; visualization, M.A.L.; supervision, A.R.M., M.G. and M.P. All authors have read and agreed to the published version of the manuscript.

Funding: This research received no external funding.

Institutional Review Board Statement: Not applicable.

Informed Consent Statement: Not applicable.

Data Availability Statement: Data are contained within this paper.

Conflicts of Interest: The authors declare no conflicts of interest.

References

1. Boyd, D.; VanGilder, B.D.; Beiting, E.J. Numerical and experimental investigations of rarefied flow in a small nozzle. *AIAA J.* **1996**, *34*, 2320–2326. [CrossRef]
2. Hatta, S.; Aso, S. Numerical studies on effect of nozzle geometry and of flow continuity on thrust performance. In Proceedings of the 27th International Electric Propulsion Conference, Pasadena, CA, USA, 15–19 October 2001; Paper 01-193.
3. Laure, S.; Heiermann, J.; Auweter-Kurtz, M.; Kurtz, H. Experimental and numerical investigation of a power augmented thermal arc jet. In Proceedings of the 37th Joint Propulsion Conference and Exhibit, Salt Lake City, UT, USA, 8–11 July 2001; AIAA Paper No. 2001-3923.
4. Jugroot, M.; Harvey, J.K. Numerical modeling of neutral and charged particles within a gridded ion thruster. In Proceedings of the 27th International Electric Propulsion Conference, Pasadena, CA, USA, 15–19 October 2001; Paper 01-100.
5. Mikellides, I.G.; Katz, I.; Goebel, D. Numerical simulation of the hollow cathode discharge plasma dynamics. In Proceedings of the 29th International Electric Propulsion Conference, Princeton, NJ, USA, 31 October–4 November 2005; Paper 05-200.
6. Boyd, I.D.; Crofton, M.W. Modeling the plasma plume of a hollow cathode. *J. Appl. Phys.* **2004**, *95*, 3285–3296. [CrossRef]

7. Blateau, V.; Martinez-Sanchez, M.; Batischev, O. A computational study of internal physics effects in a Hall thruster. In Proceedings of the 38th AIAA/ASME/SAE/ASEE Joint Propulsion Conference & Exhibit, Indianapolis, IN, USA, 7–10 July 2002; AIAA American Institute of Aeronautics and Astronautics: Reston, VA, USA, 1995; Paper No. 2002-4105.
8. González-Bárcena, D.; Peinado-Pérez, L.; Fernández-Soler, A.; Pérez-Muñoz Á, G.; Álvarez-Romero, J.M.; Ayape, F.; Sanz-Andrés, Á. TASEC-Lab: A COTS-based CubeSat-like university experiment for characterizing the convective heat transfer in stratospheric balloon missions. *Acta Astronaut.* **2022**, *196*, 244–258. [CrossRef]
9. Barnhart, D.J.; Vladimirova, T.; Sweeting, M.N. Very-small-satellite design for distributed space missions. *J. Spacecr. Rocket.* **2007**, *44*, 1294–1306. [CrossRef]
10. Helvajian, H.; Robinson, E.Y. *Micro- and Nanotechnology for Space Systems*; The Aerospace Press: Los Angeles, CA, USA, 1997.
11. Esper, J.; Panetta, P.V.; Ryschkewitsch, D.M.; Wiscombe, D.W.; Neeck, S. NASA-GSFC nano-satellite technology for earth science missions. *Acta Astronaut.* **2000**, *46*, 287–296. [CrossRef]
12. Mueller, J.; Yang, E.; Green, A.; White, V. Design and fabrication of MEMS-based micropropulsion devices at JPL. In Proceedings of the SPIE 2001 Proceedings Volume 4558, Reliability, Testing, and Characterization of MEMS/MOEMS, San Francisco, CA, USA, 21–25 October 2001; SPIE: San Francisco, CA, USA; pp. 57–71. [CrossRef]
13. Janson, S.W.; Helvajian, H.; Hansen, W.W.; Lodmell, L.J. Microthrusters for nanosatellites. In Proceedings of the Second International Conference on Integrated Micro Nanotechnology, Pasadena, CA, USA, 11–15 April 1999; The Aerospace Corporation: Pasadena, CA, USA, 1999.
14. Ellis, R.A.; Keller, R.B., Jr. *Solid Rocket Motor Nozzles*; NASA: Cleveland, OH, USA, 1975.
15. Johnston, J.R.; Signorelli, R.A.; Freche, J.C. *Performance of Rocket Nozzle Materials with Several Solid Propellants*; NASA: Cleveland, PH, USA, 1966.
16. Maisonneuve, Y. Ablation of solid-fuel booster nozzle materials. *Aerosp. Sci. Technol.* **1997**, *1*, 277–289. [CrossRef]
17. Turchi, A.; Bianchi, D.; Nasuti, F.; Onofri, M. A numerical approach for the study of the gas–surface interaction in carbon–phenolic solid rocket nozzles. *Aerosp. Sci. Technol.* **2013**, *27*, 25–31. [CrossRef]
18. Su, J.-M.; Xie, Q.; Feng, J.; Zhu, Y.; Zhang, M.; Xiao, Z.-C. Evaluation of performance and function of graphite material for throat insert. *J. Solid. Rocket. Technol.* **2015**, *38*, 554–561.
19. Nigar, B.; Dönmez, S.; Çöker, D.; Özerin, S. Understanding mechanical failure of graphite rocket nozzle throats under thermal stresses. *Aerosp. Sci. Technol.* **2021**, *119*, 107152. [CrossRef]
20. Gomaa, A.R.; Huang, H. Thermo-structural analysis of steel-composite wall nozzle. *Int. J. Model. Optim.* **2016**, *6*, 261.
21. Rovey, J.L.; Lyne, C.T.; Mundahl, A.J.; Rasmont, N.; Glascock, M.S.; Wainwright, M.J.; Berg, S.P. Review of multimode space propulsion. *Prog. Aero. Sci.* **2020**, *118*, A100627. [CrossRef]
22. Erichsen, P. Performance evaluation of spacecraft propulsion systems in relation to mission impulse requirements. In Proceedings of the Second European Spacecraft Propulsion Conference, Noordwijk, The Netherlands, 27–29 May 1997; ESA SP-398, pp. 189–194.
23. Sarritzu, A.; Lauck, F.; Werling, L.; Pasini, A. Assessment of propulsion system architectures for green propellants-based orbital stages. In Proceedings of the 73rd International Astronautical Congress, Paris, France, 18–22 September 2022; International Astronautical Federation: Paris, France, 2022.
24. Santi, M.; Fagherazzi, M.; Barato, F.; Pavarin, D. Design and testing of a hydrogen peroxide bipropellant thruster. In *AIAA Propulsion and Energy 2020 Forum*; American Institute of Aeronautics and Astronautics: Reston, VI, USA, 2020.
25. Sutton, G.P.; Biblarz, O. *Rocket Propulsion Elements*, 9th ed.; Wiley: Hoboken, NJ, USA, 2017.
26. Erichsen, P.; Wolff, P. A software tool for the performance evaluation of spacecraft propulsion systems. In Proceedings of the Third International Conference on Spacecraft Propulsion, Cannes, France, 10–13 October 2000; ESA SP, Volume 465.
27. Zakirov, V.; Zhang, H.-Y. A model for the operation of nitrous oxide monopropellant. *Aerosp. Sci. Technol.* **2008**, *12*, 318–323. [CrossRef]
28. Haworth, D.C.; Pope, S.B. Transported Probability Density Function Methods for Reynolds-Averaged and Large-Eddy Simulations. In *Fluid Mechanics and Its Applications*; Springer: Dordrecht, The Netherlands, 2011; Volume 95.